Supplementary Information

Solvent Mediated Morphology Control of Zn MOFs as Carbon Templates for Application in Supercapacitors

Jongkook Hwang,[a] Runyu Yan,[a] Martin Oschatz,[a] and Bernhard V. K. J. Schmidt[a]*

[a] Department of Colloid Chemistry, Max-Planck Institute of Colloids and Interfaces, Am Mühlenberg 1, 14476 Potsdam, Germany

Email: bernhard.schmidt@mpikg.mpg.de

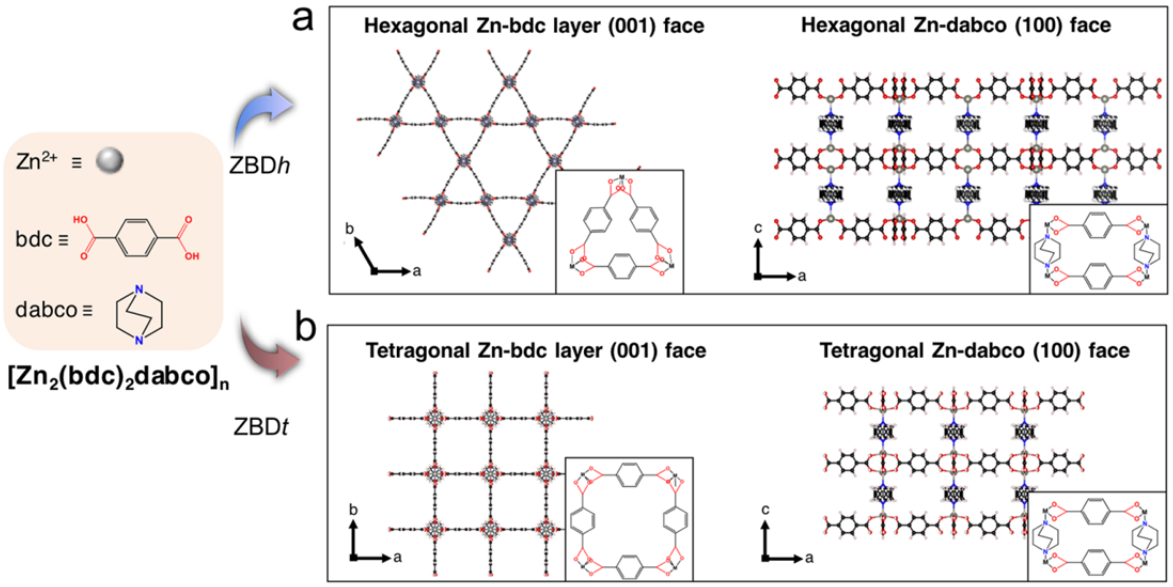

Figure S1. Two conformational isomers of $[Zn_2(bdc)_2dabco]_n$ having the same chemical composition but different framework topology.[1] (a) ZBD*h*: hexagonal framework. The 2D layers consist of triangles and hexagons, corresponding to Kagome nets. (b) ZBD*t*: tetragonal framework. The 2D layers consist of squares, corresponding to square grid nets.

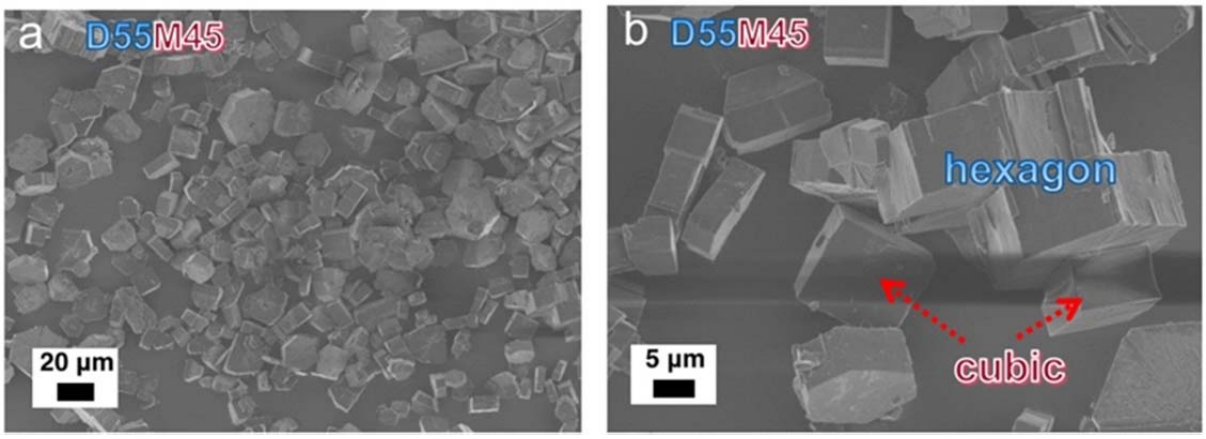

Figure S2. Intermediate mixture of ZBD*h* and ZBD*t* prepared in a cosolvent of DMF 5.5: MeOH 4.5.

Table S1. The size and aspect ratio of ZBD*h*(*t*)-D*x*M*y*.

a) Definition of aspect ratio

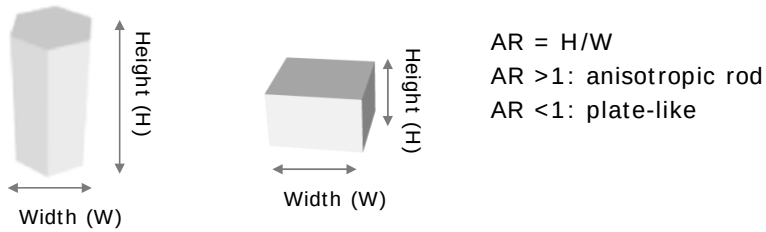

b)

Sample	Height [μm]	Width [μm]	H/W Aspect Ratio
ZBD*h*-D10	0.58 ± 0.21	0.17 ± 0.054	3.5 ±1.1
ZBD*h*-D9M1	1.2 ± 0.49	0.66 ± 0.19	2.0 ± 0.88
ZBD*h*-D7M3	8.1 ± 3.6	13 ± 3.4	0.62 ± 0.29
ZBD*h*-D6M4	40 ± 10	75 ± 12	0.53 ± 0.10
ZBD*t*-D5M5	1.4 ± 0.65	3.4 ± 1.3	0.44 ± 0.18
ZBD*t*-D3M7	0.23 ± 0.089	0.72 ± 0.19	0.32 ± 0.10
ZBD*t*-D1M9	0.19 ± 0.087	0.65 ± 0.21	0.30 ± 0.11
ZBD*t*-M10	0.12 ± 0.051	0.43 ± 0.14	0.29 ± 0.070

The height and width are defined in (a). The size was estimated by assessing 100 particles from SEM images. The particle size is defined as the size of major axis at the given condition.

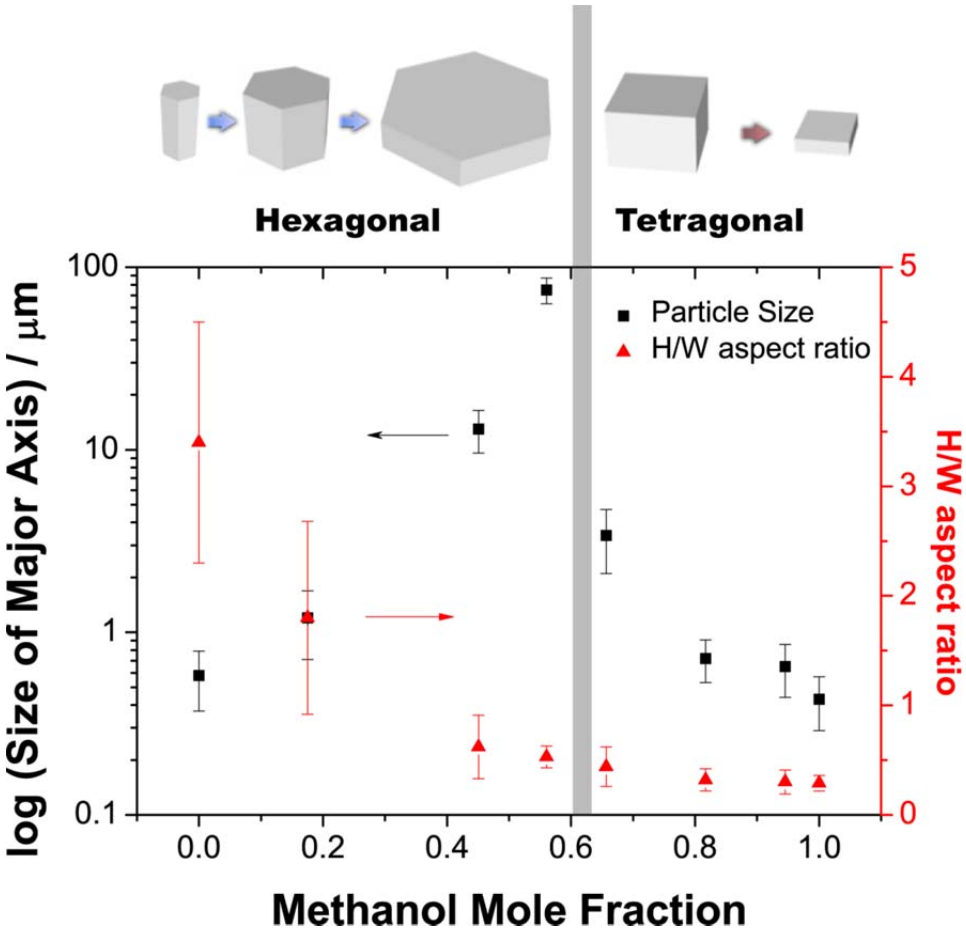

Figure S3. The changes in the particle size and H/W aspect ratio with respect to methanol mole fractions.

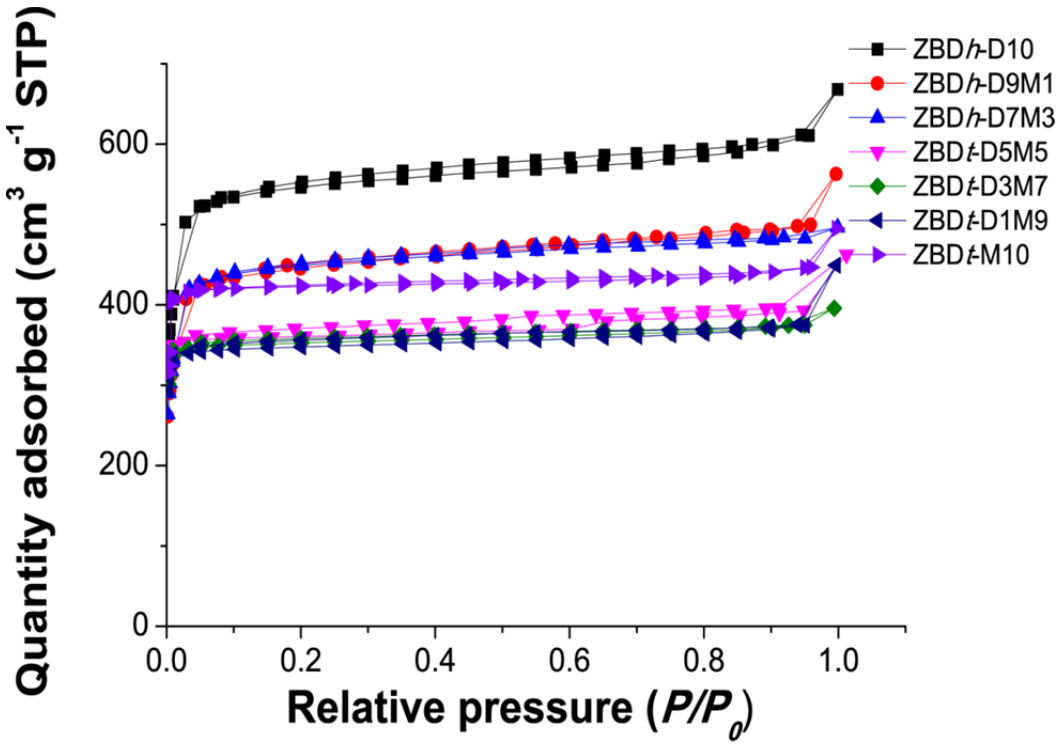

Figure S4. N_2 sorption isotherms for all ZBD*h*(*t*)-D*x*M*y*.

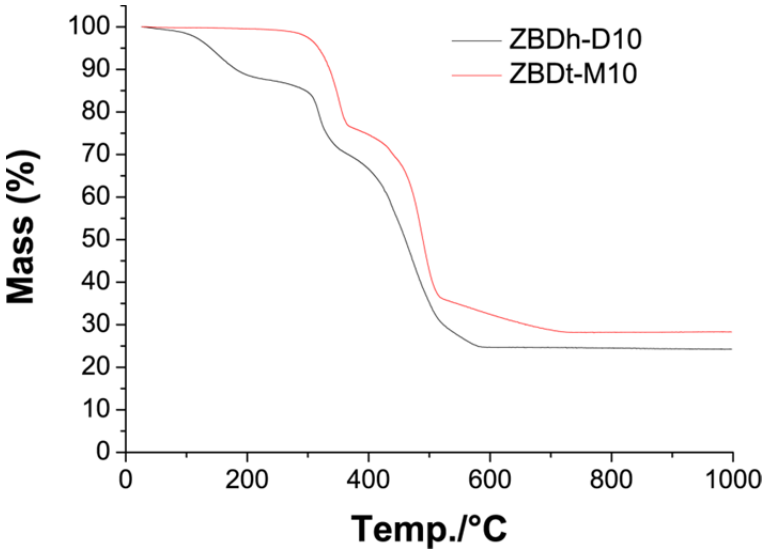

Figure S5. TGA profiles of representative ZBD*h*-D10 and ZBD*t*-M10 under constant artificial air flow at a heating rate of 10 °C min^{-1} to 1000 °C.

The synthesized ZBDs were washed with DMF or MeOH and dried under vacuum at 85 °C before materials characterization. The volatile MeOH in as-made ZBD*t*-M10 can be removed relatively easily by evacuation at 85 °C, therefore, the estimated mass loss from MeOH removal is very small in ZBD*t*-M10. In contrast, substantial weight ~ 14% of DMF still included in ZBD*h*-D10 after evacuation at 85 °C because of high boiling point of DMF. Both ZBDs lose the guest solvents < 200 °C, and are thermally stable up to 300 °C, which is consistent with their bulk counterparts reported in literature. [2, 3]

Table S2. Physicochemical properties of ZBD*h*(*t*)-D*x*M*y*.

D: M v/v ratio	**D: M Mole ratio**	**Surface area [a] [m^2/g]**	**Pore size [b] [nm]**	**Topology**	**Morphology [e]**
D10	D10	2160	1.3, 1.6	kgm[c]	hexagonal nanorods
D9M1	D8.25 M1.75	1920	1.3, 1.6	kgm	hexagonal microrods
D7M3	D5.5 M4.5	1880	1.3, 1.6	kgm	hexagonal microplates
D6M4	D4.4 M5.6	1900	1.3, 1.6	kgm	hexagonal microplates
D5.5M4.5	D3.9 M6.1	1650	1.1-1.6	kgm, sql	intermediate mixture
D5M5	D3.4 M6.6	1540	1.1	sql[d]	tetragonal microcube
D3M7	D1.8 M8.2	1500	1.1	sql	tetragonal microplate
D1M9	D0.55 M9.45	1480	1.1	sql	tetragonal nanoplate
M10	M10	1760	1.1	sql	tetragonal nanoplate

[a] Determined by BET method. [b] Determined by a slit pore NLDFT equilibrium model. [c] Kagome net, determined by PXRD [d] Square grid net, determined by PXRD. [e] Observed by SEM.

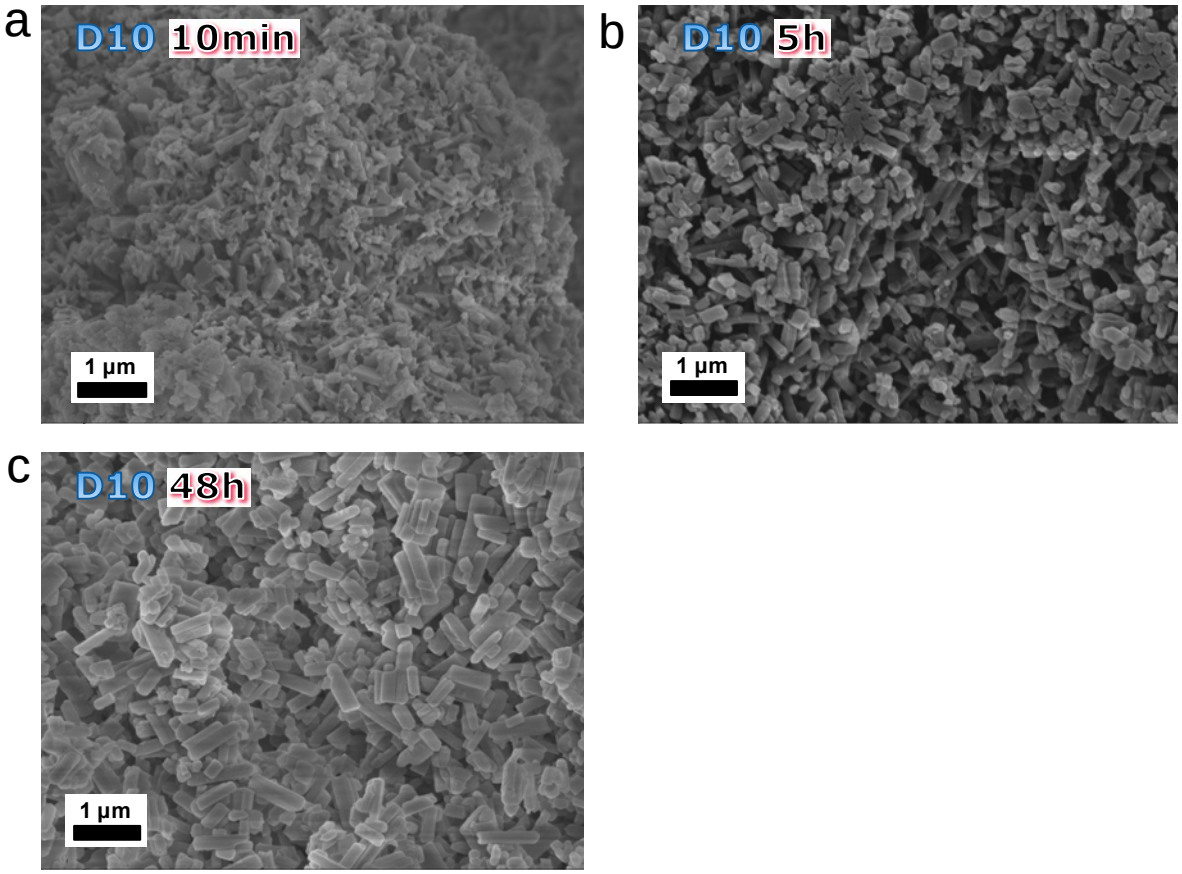

Figure S6. Time dependent SEM observation of ZBD*h*-D10 growth.

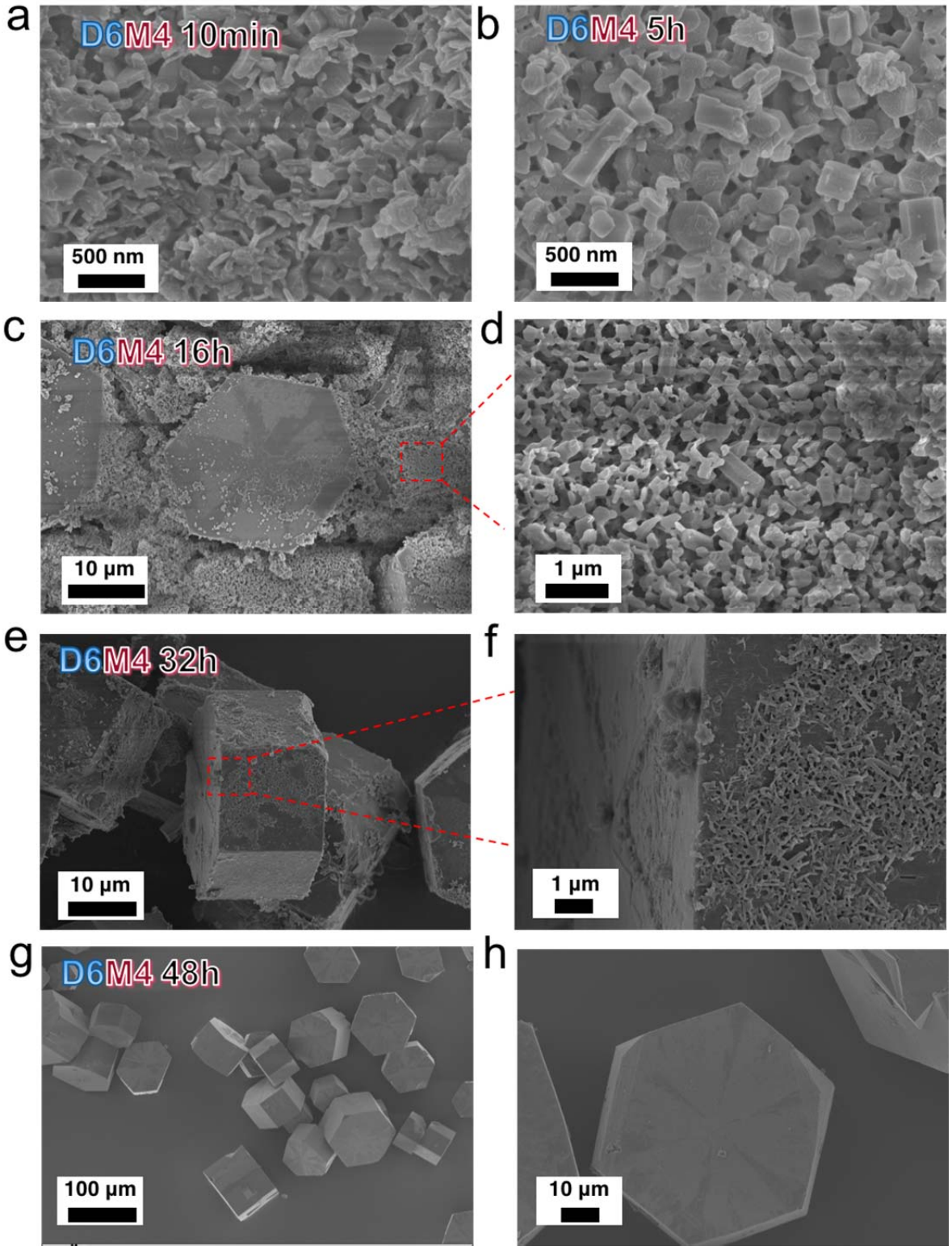

Figure S7. Time dependent SEM observation of ZBD*h*-D6M4 growth.

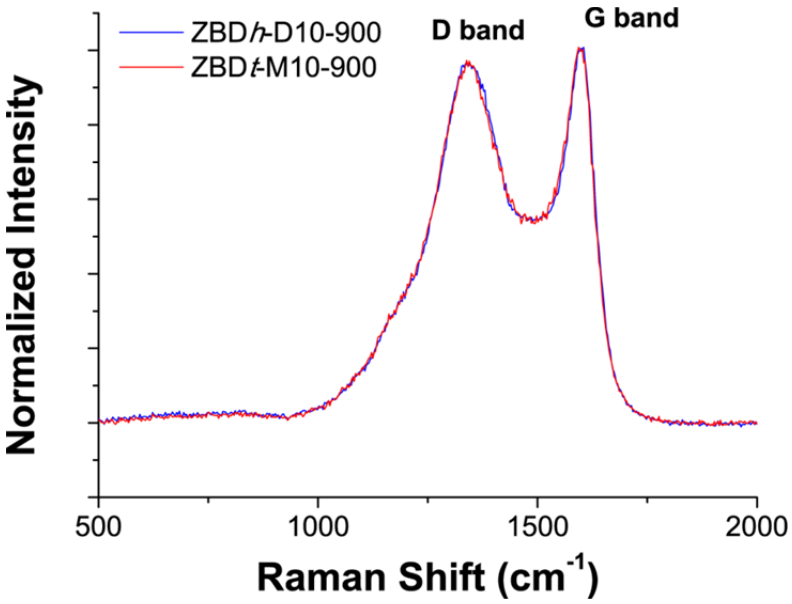

Figure S8. Raman spectra of ZBD-derived carbon.

Table S3. ICP and CHN results of ZBD-derived carbons.

Carbon	Zn content [wt%][a]	C [wt%][b]	H [wt%][b]	N [wt%][b]
ZBD*h*-D10-900	0.032	86.9	2.95	4.15
ZBD*t*-M10-900	0.026	85.8	3.05	4.13

[a] Determined by ICP-OES. [b] Determined by CHN microanalysis.

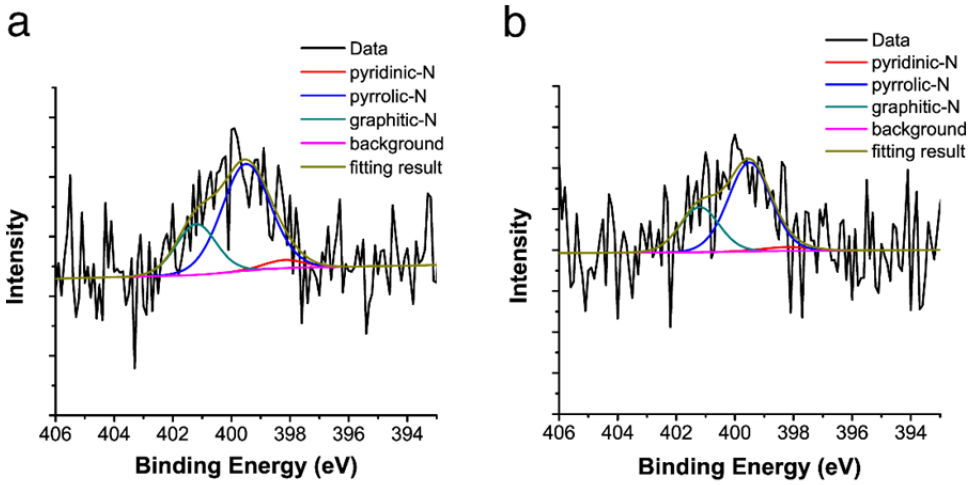

c

Carbon	Pyridinic N [%]	Pyrrolic N [%]	Graphitic N[%]
ZBD*h*-D10-900	4.2	68.8	27.0
ZBD*t*-M10-900	3.4	65.9	30.7

Figure S9. Deconvoluted N1s XPS spectra of ZBD*h*-D10-900 (a) and ZBD*t*-M10-900 (b) and relative proportion of bonding configuration of N species (c).

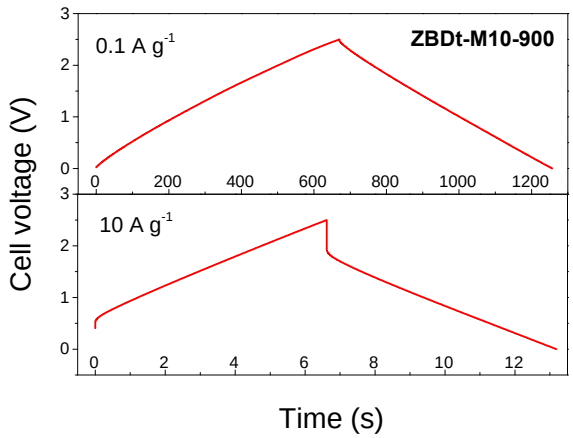

Figure S10. Galvanostatic charging/discharging curve of ZBDt-M10-900 at 0.1 A g^{-1} and 10 A g^{-1}.

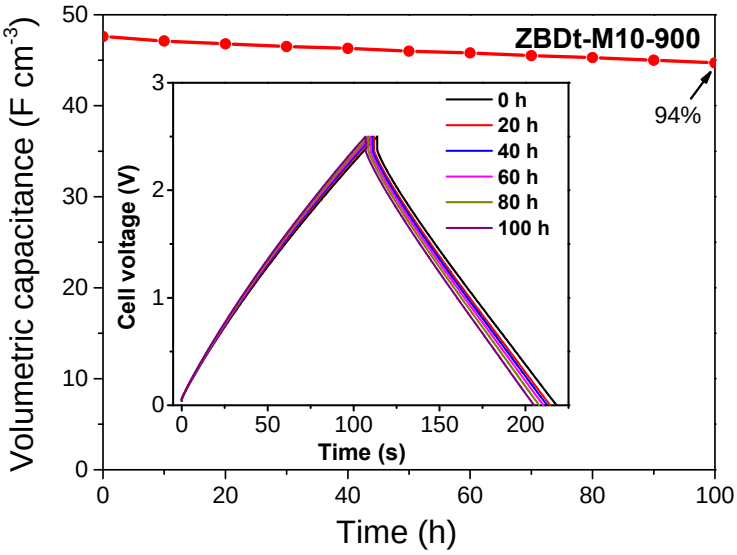

Figure S11. Foating test of the EDLC cell with ZBD*t*-M10-900 as the electrodes for 100 h floating at 2.5 V.

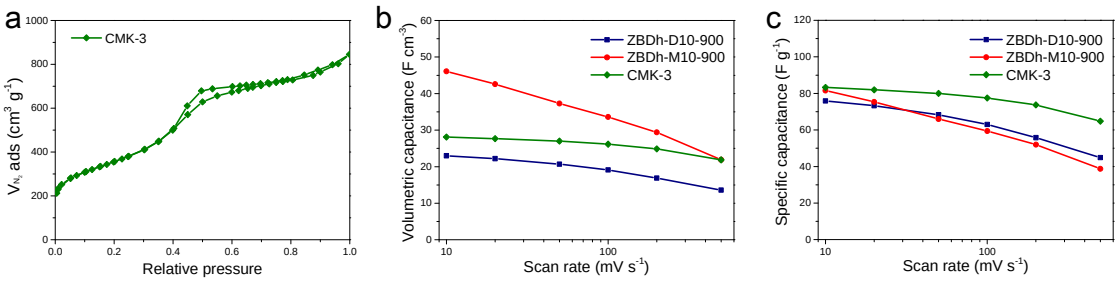

Figure S12. (a) N_2 physisorption isotherms of CMK-3. (b) Volumetric and (c) gravimetric capacitance retention with the increase of scan rate of the prepared three carbon samples.

Table S4. Capacitances of the representative MOF-derived carbons and typical carbon materials.

Material	Template or precursor	Electrolyte	Scan rate	F g^{-1}	F cm^{-3}	Ref.
MOF derived carbons in aqueous electrolyte						
NPC	MOF-5 and furfuryl alcohol	1 M H_2SO_4	5 mV s^{-1}	204	80	S4
NPC_{650}	MOF-5 and furfuryl alcohol	1 M H_2SO_4	5 mV s^{-1}	167	84	S5
MPC-A	MOF-5 and phenolic resin, KOH activation	6M KOH	2 mV s^{-1}	196	81	S6
C1000	ZIF-8 and furfuryl alcohol	1 M H_2SO_4	5 mV s^{-1}	161	52	S7
Z-900	ZIF-8	1 M H_2SO_4	2 mV s^{-1}	214	200	S8
C-S1900	Fe based coordination polymer	6M KOH	2 mV s^{-1}	70	n/a	S9
MOF derived carbons in organic electrolyte						
MAC-A	MOF-5, carbon tetrachloride and ethylenediamine, KOH activation	1.5 M Et4NBF_4/AN	2 mV s^{-1}	156	145	S6
NPC	ZIF-8	2 M NEt_4BF_4/PC	10 mV s^{-1}	21	9.24	S10
ZBD*t*-M10-900	ZBD*t*	1 M $TEABF_4$/AN	10 mV s^{-1}	80	46	This work
State of the art carbon materials in organic electrolyte						
AC	pollen	$EMIMBF_4$	1 A g^{-1}	207	104	S11
N-doped AC	peptides of silk fibroins	1 M $TEABF_4$/PC	1 mA cm^{-2}	52	25	S12
Cu modified AC	Cu nanocrystal and commercial AC	TEATFB	0.20 A g^{-1}	79	62	S13
Functionalized Graphene	Graphite oxide, $Mg(OH_2)$ nanosheets as templates	1 M $TEABF_4$/AN	0.50 A g^{-1}	103	80	S14
CDC	Ta_4HfC_5 and $WTiC_2$ derived carbon	1 M $TEMABF_4$/AN	1 mV s^{-1}	116	75	S15
A-CNTs	Aligned CNT via CVD	3 M $EMIBF_4$/PC	0.10 A g^{-1}	260	130	S16
RGO/AC	Organogels of graphene and AC	1 M $TEABF_4$	1.0 A g^{-1}	117	20	S17

References

S1. M. Kondo, Y. Takashima, J. Seo, S. Kitagawa and S. Furukawa, *CrystEngComm*, 2010, **12**, 2350-2353.

S2. D. N. Dybtsev, H. Chun and K. Kim, *Angew. Chem., Int. Ed.*, 2004, **43**, 5033-5036.

S3. H. Chun and J. Moon, *Inorg. Chem.*, 2007, **46**, 4371-4373.

S4. B. Liu, H. Shioyama, T. Akita and Q. Xu, *J. Am. Chem. Soc.*, 2008, **130**, 5390.

S5. B. Liu, H. Shioyama, H. Jiang, X. Zhang and Q. Xu, *Carbon* 2010, **48**, 456.

S6. J. Hu, H. Wang, Q. Gao and H. Guo, Carbon, 2010, 48, 3599.

S7. H.-L. Jiang, B. Liu, Y.-Q. Lan, K. Kuratani, T. Akita, H. Shioyama, F. Zong and Q. Xu, *J. Am. Chem. Soc.*, 2011, **133**, 11854.

S8. W. Chaikittisilp, M. Hu, H. Wang, H.-S. Huang, T. Fujita,K. C.-W. Wu, L.-C. Chen, Y. Yamauchi and K. Ariga, *Chem. Commun*., 2012, **48**, 7259.

S9. P. Su, L. Jiang, J. Zhao, J. Yan, C. Li, Q. Yang, *Chem. Commun*. 2012, **48**, 8769.

S10. R. R. Salunkhe, C. Young, J. Tang, T. Takei, Y. Ide, N. Kobayashia, Y. Yamauchi, *Chem. Commun*., 2016, **52**, 4764.

S11. L. Zhang, F. Zhang, X. Yang, K. Leng, Y. Huang and Y. S. Chen, *Small*, 2013, **9**, 1342.

S12. Y. J. Kim, Y. Abe, T. Yanagiura, K. C. Park, M. Shimizu,T. Iwazaki, S. Nakagawa, M. Endo and M. S. Dresselhaus, *Carbon*, 2007, **45**, 2116.

S13. L. L. Zhang, S. L. Candelaria, J. J. Tian, Y. W. Li,Y. X. Huang and G. Z. Cao, *J. Power Sources*, 2013, **236**, 215.

S14. J. Yan, Q. Wang, T. Wei, L. Jiang, M. Zhang, X. Jing and Z. Fan, *ACS Nano*, 2014, **8**, 4720.

S15. I. Tallo, T. Thomberg, H. Kurig, K. Kontturi, A. Janes and E. Lust, *Carbon*, 2014, **67**, 607.

S16. Y. Zhou, M. Ghaffari, M. Lin, E. M. Parsons, Y. Liu, B. L. Wardle and Q. M. Zhang, *Electrochim. Acta*, 2013, **111**, 608.

S17. Q. Q. Zhou, J. Gao, C. Li, J. Chen and G. Q. Shi, *J. Mater.Chem. A*, 2013, **1**, 9196–9201.